APL Materials

Tuning ZnO nanorods photoluminescence through atmospheric plasma treatments

Cite as: APL Mater. **7**, 081111 (2019); https://doi.org/10.1063/1.5110984
Submitted: 22 May 2019 . Accepted: 24 July 2019 . Published Online: 15 August 2019

Shujie You, Alessandro Patelli, Pedram Ghamgosar, Tiziana Cesca, Francesco Enrichi, Giovanni Mattei, and Alberto Vomiero

AIP Publishing

Tuning ZnO nanorods photoluminescence through atmospheric plasma treatments

Cite as: APL Mater. 7, 081111 (2019); doi: 10.1063/1.5110984
Submitted: 22 May 2019 • Accepted: 24 July 2019 •
Published Online: 15 August 2019

Shujie You,[1,a] Alessandro Patelli,[2,a] Pedram Ghamgosar,[1] Tiziana Cesca,[2] Francesco Enrichi,[1,3] Giovanni Mattei,[2] and Alberto Vomiero[1,3,a]

AFFILIATIONS

[1] Division of Materials Science, Department of Engineering Sciences and Mathematics, Luleå University of Technology, 97187 Luleå, Sweden
[2] Department of Physics and Astronomy, University of Padova, 35131 Padova, Italy
[3] Department of Molecular Sciences and Nanosystems, Ca' Foscari University of Venice, Via Torino 155, 30172 Venezia Mestre, Italy

[a] **Authors to whom correspondence should be addressed:** shujie.you@ltu.se; alessandro.patelli@unipd.it; alberto.vomiero@ltu.se; and alberto.vomiero@unive.it

ABSTRACT

Room temperature atmospheric plasma treatments are widely used to activate and control chemical functionalities at surfaces. Here, we investigated the effect of atmospheric pressure plasma jet (APPJ) treatments in reducing atmosphere (Ar/1‰ H_2 mixture) on the photoluminescence (PL) properties of single crystal ZnO nanorods (NRs) grown through hydrothermal synthesis on fluorine-doped tin oxide glass substrates. The results were compared with a standard annealing process in air at 300 °C. Steady-state photoluminescence showed strong suppression of the defect emission in ZnO NRs for both plasma and thermal treatments. On the other side, the APPJ process induced an increase in PL quantum efficiency (QE), while the annealing does not show any improvement. The QE in the plasma treated samples was mainly determined by the near band-edge emission, which increased 5–6 fold compared to the as-prepared samples. This behavior suggests that the quenching of the defect emission is related to the substitution of hydrogen probably in zinc vacancies (V_{Zn}), while the enhancement of UV emission is due to doping originated by interstitial hydrogen (H_i), which diffuses out during annealing. Our results demonstrate that atmospheric pressure plasma can induce a similar hydrogen doping as ordinarily used vacuum processes and highlight that the APPJ treatments are not limited to the surfaces but can lead to subsurface modifications. APPJ processes at room temperature and under ambient air conditions are stable, convenient, and efficient methods, compared to thermal treatments to improve the optical and surface properties of ZnO NRs, and remarkably increase the efficiency of UV emission.

I. INTRODUCTION

ZnO is long known as an environmentally friendly wide bandgap semiconductor with an exciton binding energy of 60 meV.[1,2] The high exciton binding energy ensures that excitonic emission is significant at room temperature, and therefore, ZnO is a promising candidate for stable room temperature luminescent and lasing devices.[3,4] ZnO with various morphologies, such as bulk ZnO, nanoparticles, films, nanowires, and tetrapods, has been extensively investigated for different applications.[5–8] Among all morphologies, the one-dimensional (1D) ZnO nanorods (NRs) and nanowires (NWs) are the most common and studied structures. The high aspect ratio in ZnO NRs and NWs makes it possible to separate the length scales for light absorption and exciton diffusion; indeed, an optimized configuration for the solar harvesting devices could be obtained with a thick absorbing layer, to maximize energy collection, and small interwire spacing for improved optical density and, hence, more efficient current generation.[3,9]

High quality ZnO NWs have been successfully synthesized using vapor phase synthesis such as chemical vapor deposition (CVD), physical vapor deposition (PVD), molecular beam epitaxy (MBE), and pulsed laser deposition (PLD). Another widely used method to produce 1D ZnO nanomaterials is hydrothermal synthesis.[10,11] Compared to vapor phase synthesis, hydrothermal

synthesis has significant advantages, including lower cost and no need of vacuum atmosphere, and therefore, it holds potential for large scale production. However, due to the low temperature and solution phase synthesis, hydrothermally grown 1D ZnO products have more crystalline defects than others, primarily due to oxygen vacancies.[12] Post-treatments are often applied to improve the quality of the hydrothermally synthesized ZnO nanowires. Even at low temperatures, indeed, zinc vacancies (V_{Zn}) can be recovered since V_{Zn} become mobile at temperatures higher than 540 K, while oxygen vacancies V_O^{2+} and V_O^0 are annealed at 650 K and 900 K,[13] respectively. It is worth noting that the optical properties of different ZnO nanostructures may be very different in terms of defect emission intensities and decay times. No correlation was found between the PL lifetimes and the defect emission intensities and positions. The near band-edge UV emission has very short lifetimes (from tens of picoseconds to nanoseconds), which are most likely due to non-radiative defects correlated with the crystalline quality and do not contribute to the visible emission.[14–17]

An alternative post-treatment able to reduce the green emissions due to ZnO NW defects is the exposure to vacuum plasma using a hydrogen-containing process gas. In this case, the vacancies are filled by hydrogen, which diffuses through the ZnO crystal.

The hydrogen passivation and doping of the crystal lead to a reduction in the visible band emission, to an increase in the near band-edge emission (NBE) at about 380 nm, and to an increase in the conductivity.[18] The doping also reduces the depletion width close to the surfaces due to the trapping of free electrons at the surface states by increasing the electron concentration.[19]

The use of process gases containing oxygen or nitrogen does not allow us to achieve results similar to hydrogen in the visible band emission reduction and NBE increase. In this case, the plasma effect is limited to the surface and no gas species diffusion in the ZnO crystals can easily be achieved.[20,21] The hydrogen doping, stable at room temperature, is reversible after a heat treatment at 500 °C, which causes hydrogen to migrate out of the ZnO crystals.

No data are present in the literature on the effect of similar plasma post-treatments performed at atmospheric pressure on ZnO NWs. However, on aluminum-doped ZnO (AZO) films, an increase in conductivity can be obtained after film exposure to an atmospheric pressure plasma using hydrogen containing process gases.[22] The conductivity increase is due to the diffusion of hydrogen few tens of nanometers at the small grain boundaries of AZO, leading to passivation of the surface defects and to an increase in carrier concentration.

In this work, we report a simple room temperature atmospheric pressure plasma jet (APPJ) treatment, using a reducing process gas, on hydrothermally synthesized ZnO NRs vertically grown on fluorine-doped tin oxide (FTO) conductive glass substrates. The optical performances of APPJ-treated ZnO NRs were improved, and the possible mechanism was studied and compared with the as-prepared and thermally treated ones.

II. EXPERIMENTAL

A. Synthesis of ZnO NRs

ZnO NRs were synthesized using the hydrothermal method, according to Ref. 23. First, a seed layer of ZnO was prepared by spin coating 0.01M zinc acetate/ethanol solution on FTO conductive glass. The FTO substrates were then annealed at 450 °C for 1 h at an ambient atmosphere to form the seed layer. The seeded substrates were put in a Teflon lined autoclave and immersed in a mixture of 100 mM Zn $(NO_3)_2{\cdot}6H_2O$ and 100 mM hexamethylenetetramine (HMTA). The substrates were placed with the conductive side (with the seeded ZnO layer) down to avoid the precipitation of ZnO aggregates on the surface which may hinder the growth of NRs. The autoclave was heated at 95 °C for 3 h. After the hydrothermal synthesis, the ZnO NR samples were washed thoroughly with distilled water and dried in air to remove the rest of the reagents.

B. APPJ post-treatment on ZnO NRs

The plasma treatment under atmosphere conditions was performed by an APPJ (Stylus Plasma Noble, Nadir srl)[24] mounted on a plotter on the as-prepared ZnO NRs/FTO samples (AS-ZnO NRs). The jet outlet was positioned at 12 mm in order to avoid the direct plasma contact with the sample. The device has an outlet orifice of 3 mm and during the treatment was moved on a raster with a step of 1 mm at a speed of 300 mm/s. A series of samples were produced as a function of the number of raster's passes on the sample surface: from 1 to 50. In order to evaluate effects that occur taking the process to the limit, an additional sample was produced by rastering the surface through 100 passes with a jet to surface distance of 2 mm. The APPJ was used in RF mode with a forward power of 20 W. The APPJ is characterized by its low processing temperature,[25] and no heating was measured on the surface after the treatment (<35 °C). The process gas was argon (purity 99.999%) at 5 slm with the addition of 6 sccm of H_2 (purity 99.999%). A nitrogen gas shell around the plasma was introduced to avoid ambient air interactions during the treatment. The stability of the plasma treatment effects was checked as a function of time during annealing in air at 300 °C for 1 h. For comparison, some of the as-prepared samples, not treated with plasma, were annealed at 300 °C for 1 h in an ambient atmosphere to compare with the plasma treatment (Ann-ZnO NRs).

C. Sample characterizations

The morphology of the ZnO NRs was characterized using a Magellan 400 scanning electron microscope (SEM) from the FEI company. X-ray diffraction (XRD) patterns were recorded through a PANalytical Empyrean diffractometer using Cu Kα radiation. Raman spectra were acquired using a Senterra Raman spectrometer with 1200 groove/mm grating under 532 nm laser excitation. To have a solid benchmark on PL measurements, steady-state PL analyses were carried out using two different systems: a FLS980 high-resolution spectrometer from Edinburgh Instruments and a HORIBA FluoroMax spectrofluorometer; in both systems, the samples were excited at 325 nm with a monochromatized broadband Xe lamp. Prior to the PL measurements, the samples were cleaned with 5 min UV exposure.

A 275 nm UV Edinburgh Instruments pulsed light emitting diode (EPLED) with a pulse width of about 730 ps was used for excitation during the measurement of the lifetime of ZnO UV emission at 376 nm. The PL quantum efficiency (QE, η) was measured using the Edinburgh FLS980 spectrometer equipped with an integrating sphere.

The QE of ZnO/FTO samples was calculated by the following equation:

$$\eta = \frac{E_B - E_A}{S_A - S_B}, \quad (1)$$

where S_A and S_B are the scatterings of excitation from a bare FTO substrate and the ZnO NRs/FTO samples, while E_A and E_B are the emissions from FTO and ZnO NRs/FTO samples, respectively. E_A(FTO) is strong compared to E_B(ZnO/FTO), as shown in Fig. SI-1. However, the typical E_A(FTO) spectra, for example, the three sharp peaks at 593, 615, and 685 nm, did not show up in the E_B(ZnO/FTO) spectra. Therefore, we consider that ZnO NRs are dense and thick enough to absorb most of the incoming excitation, so that FTO was barely exposed to excitation and thus its contribution E_A is negligible in QE calculation.

III. RESULT AND DISCUSSION

A. Morphology and structural properties

In Table I, the list of analyzed samples is collected. We varied in this study the number of passes on the whole sample area of the APPJ from 1 to 50. The plasma parameters were maintained constant, with a jet/sample distance of 12 mm to avoid plasma contact with the sample surface and using argon as the process gas with the addition of a small percentage ~1 ‰ of hydrogen. A sample with 100 passes at a jet/sample distance of 2 mm was produced to show the effects taking the process to its limit with the setup used. In Fig. 1, the SEM images indicate that both the as-prepared and plasma treated ZnO NRs have hexagonal cross-sections with diameter 50–70 nm and length around 1 μm, as it is typical for single crystalline NRs.[26] The ZnO NRs are mostly vertically aligned and slightly tapered. The morphology of ZnO NRs did not change after the plasma treatment.

XRD patterns [Fig. 1(d)] showed that all the samples exhibited very sharp and strong diffraction at 2θ=36.5°, which indicates a single crystal structure of the single NRs, as expected from SEM, and their strong preferred orientation along the (002) plane. Such behavior is well documented in the literature for single crystalline oriented ZnO NR arrays in which the relative intensity of the peaks differs substantially from ZnO powders, due to the preferential orientation of the crystalline domains in oriented arrays of single crystals.[27,28] Neither the relative intensity nor the peak position changed after the APPJ treatment except for a small broadening of the strongest (002) diffraction in the P-100 sample [orange curve in Fig. 1(e)], which might be due to the interstitial hydrogen induced lattice relaxation.[1]

Figure 1(f) shows the typical Raman spectrum of AS-ZnO NRs, consisting of two intense Raman peaks at 99 and 437 cm^{-1}, which are associated with the vibration of the heavy Zn sublattice ($E_{2\text{-low}}$) and oxygen atoms ($E_{2\text{-high}}$), respectively,[29] and a third weaker peak at around 330 cm^{-1}, which is related to second-order Raman processes, $E_{2\text{-low}}-E_{2\text{-high}}$ vibration mode. The Raman spectra of plasma treated samples coincide with those of Ann-ZnO NRs and are identical to those of AS-ZnO NRs [Fig. 1(f)]. No peak shift or appearance of new peaks was observed after the plasma treatment. This indicates that the room temperature APPJ process and the annealing at 300 °C do not appreciably modify the structure of ZnO NRs. The Raman line at 570–580 cm^{-1}, which is often correlated with defects in ZnO powders and thin films,[30] is not observed in all the AS-ZnO and treated samples.

B. Steady-state photoluminescence

Steady-state photoluminescence is usually used to examine the quality of ZnO crystals and to highlight the effects of the post-treatments.[29] In this study, all the as-prepared ZnO-NR samples showed two emission bands under 325 nm excitation (Fig. SI-2): a sharp UV-emission centered at 376 nm (usually called near band-edge emission, NBE) and a broad visible emission between 450 nm and 750 nm (usually considered to be defect related emission and indicated as deep-level emission, DLE). The NBE of ZnO at room temperature is attributed to the free-exciton recombination, while the visible emission is related to defects. It is still being debated in the literature if their cause is the oxygen or the zinc vacancy (V_O or V_{Zn}).[13,31,32]

The relative intensity of NBE and DLE (I_{NBE}/I_{DLE}) is related to the synthesis methods, annealing temperature, aspect ratio of NRs, and measuring conditions.[33] For example, it has been reported that the I_{NBE}/I_{DLE} in ZnO nanoparticles with an average diameter of 20 nm increases from 0.15 to 1.72 when the aspect ratio increases from 1 to 5.[34]

The ZnO NRs in this study had an average diameter of 50–70 nm and an aspect ratio in the range of 10–20. The PL of the as-prepared samples differed by no more than 10% in the whole measured wavelength range within the series, ensuring that the

TABLE I. List of the analyzed samples.

	Name	Process gas	Passes	Distance (mm)
As-prepared	AS-ZnO NRs			
Annealed	Ann-ZnO NRs	Air/300 °C/1 h		
	P-1	Ar + H_2	1	12
	P-5[a]	Ar + H_2	5	12
APPJ	P-10	Ar + H_2	10	12
	P-50	Ar + H_2	50	12
	P-100	Ar + H_2	100	2

[a]The sample P-5 undergoes annealing at 300 °C for 1 h after plasma treatment, according to Sec. II. The P-5 after annealing is labeled P-5-Ann. The PL properties of P-5 are recorded both after plasma treatment and after annealing (see the main text).

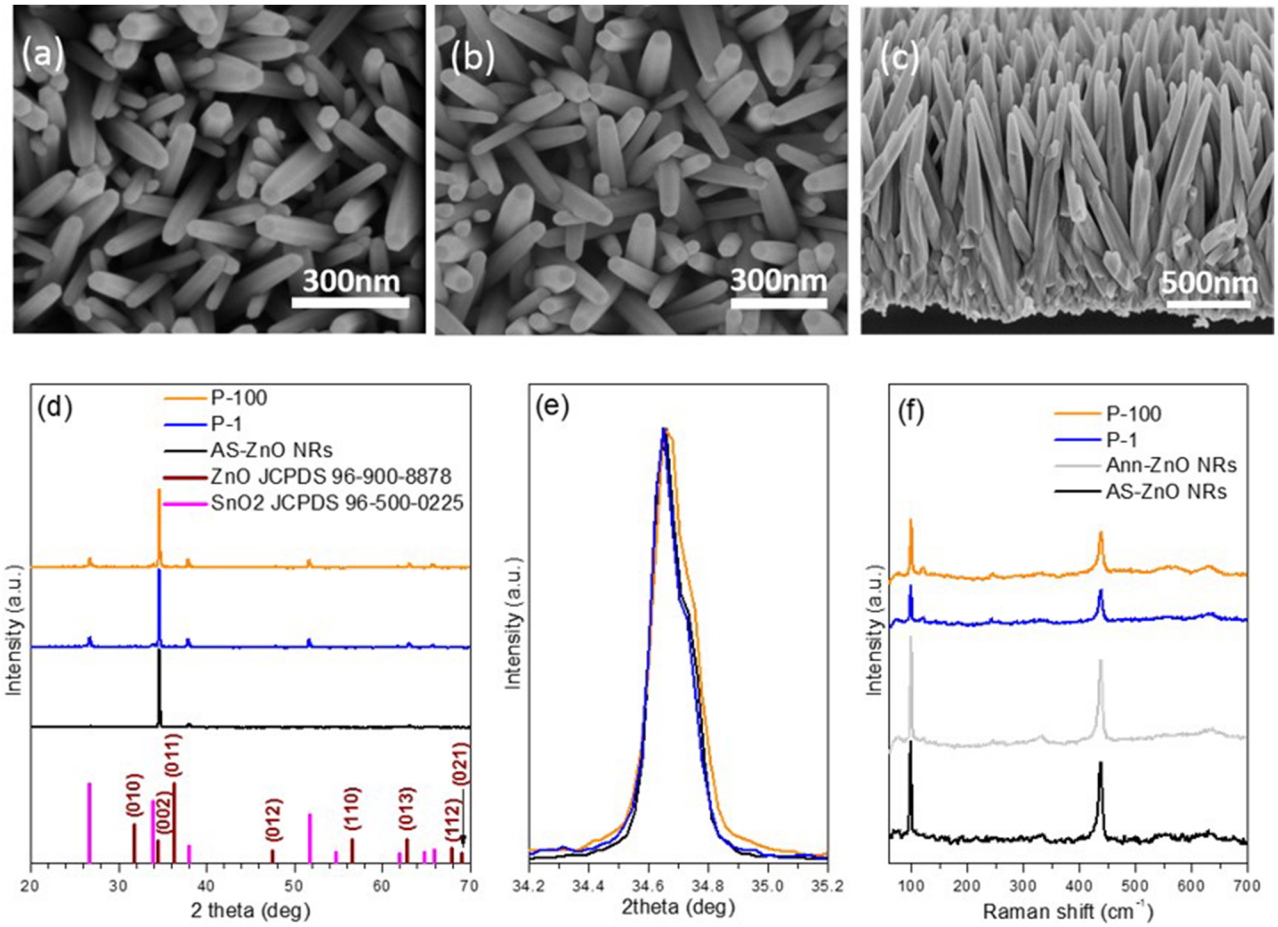

FIG. 1. [(a)–(c)] SEM images of ZnO NRs: (a) before (sample AS-ZnO NRs) and (b) after plasma treatment (sample P-1). In (c), the cross-sectional SEM of the sample AS-ZnO NRs is reported. (d) XRD patterns of various samples and (e) expanded view of the patterns in the region of the (002) diffraction peak. (f) Raman spectra of As-ZnO NRs, after annealing and APPJ treatments.

production process was reproducible and the samples were comparable (Fig. SI-2). In the plasma treated samples [Fig. 2(a)], the NBE of all the samples showed an increase compared to that of the as-prepared ones and a corresponding decrease in the DLE. The relative intensity ratio I_{DLE}/I_{NBE} reduced from about 50% in the as-prepared to less than 5% in the treated ones. The samples undergoing many passes in plasma reducing atmosphere (P-5, P-15, and P-50) showed an asymmetric broadening of the NBE band in the visible side, while the DLE band is remarkably quenched.

Since no morphologies or crystal changes could be observed by SEM, XRD, or Raman spectroscopy, the changes of the optical properties have to be linked only to point defect recovery and band structure changes.

As already documented in the literature, the exposure of ZnO to H_2 vacuum plasma could induce hydrogen atoms penetrating into the ZnO structure since hydrogen is a fast interstitial diffuser in ZnO even at low temperatures.[20] The penetration depth of hydrogen could include the full NR volume.[35] The H_2 incorporation may improve the quality of ZnO NRs in two ways:

Path (1) Hydrogen passivates the recombination centers in ZnO NRs. The DLE caused by V_O and V_{Zn} related defects is passivated by trapping hydrogen, respectively, in a Vo-H complex (or H_o), resulting in a shallow donor bound or in a V_{Zn}-H_2 complex which has no electronic levels in the gap.[36] The complexes are stable up to 400–500 °C.[13] The hydrogen can also combine with the hydroxyl groups present in the ZnO NRs and lead to water desorption.[37] Both cases improve the electron-hole recombination and thus lead to an increase in the UV-emission in PL spectra.[38] The stronger increase in the NBE intensity after just 1 pass in the plasma treatment relative to the annealing process may suggest that these passivation and water desorption processes involve a higher volume due to hydrogen diffusion.

Path (2) Hydrogen atoms can easily diffuse into the ZnO structure also in interstitial sites leading to a H_i n-doping in ZnO NRs and also behaving as a shallow donor.[39] H_i is mainly responsible for the improved conductivity after the plasma treatments. At the same time, it is much less stable compared to vacancy complexes and it was reported to desorb even at about 300 °C.[38]

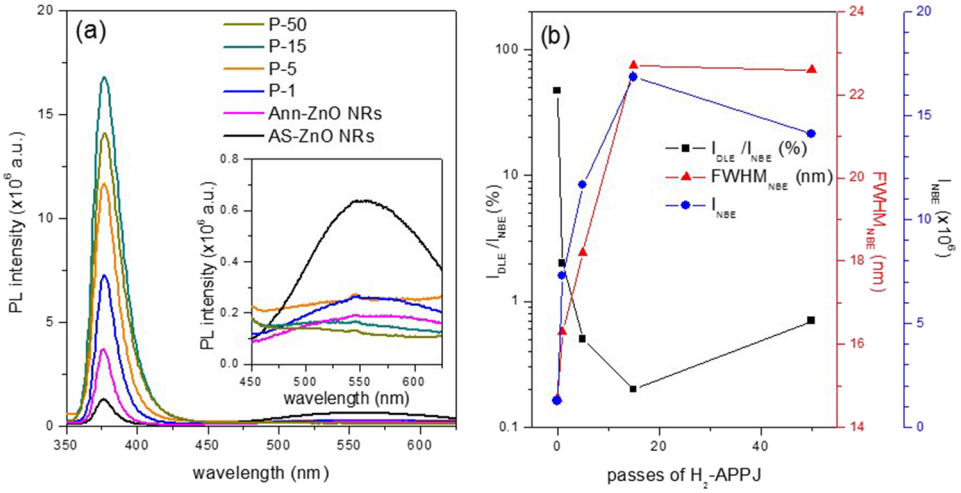

FIG. 2. (a) Steady-state PL of the as-prepared, thermally annealed, and APPJ treated ZnO NRs (the spectra were recorded using the HORIBA Fluoro-Max spectrofluorometer); the inset of (a) shows the expanded view of the DLE region. (b) Relative intensity and FWHM of PL vs the number of passes of APPJ treated samples.

Our results are coherent with the literature, suggesting that also at atmospheric pressure, the plasma treatment allows us to obtain hydrogen incorporation inside the ZnO crystals, with a process in the time scale of milliseconds. Even in the sample P-1, where the NR exposure to plasma can be estimated at less than 100 ms, the DLE is reduced to one third with respect to AS-ZN-O NRs and to lower values with respect to Ann-ZnO NRs. The low temperature of the annealing suggests that the main origin of the DLE was the V_{Zn}, which have a lower energy mobility barrier. Moreover, the DLE, which is probably the combination of several contributions, is centered to low energy values, at about 2.14 eV, usually attributed to V_{Zn}.[40,41] The hydrogen diffusing in the NRs forms the complexes at the point defect sites, reducing gradually the deep levels in the energy gap. The DLE indeed decreases as a function of the passes, and at the same time, the NBE intensity and the FWHM increase. The asymmetric NBE broadening can be due to violet emission centers caused by the bound exciton states created by hydrogen incorporation.[42] In this case, it coherently follows the increase of hydrogen doping as a function of the number of passes.

However, the intensity of the NBE did not show a monotonic trend as a function of the number of passes. The single pass plasma treatment in the Ar-H_2 atmosphere resulted in a fivefold increase in the NBE intensity. The NBE intensity was further increased by increasing the number of passes, recording a maximum after 15 passes with 12-fold enhancement in I_{NBE}. Samples treated with more than 15 passes showed similar NBE peak profiles with lower enhancement in the intensity. A contribution to the increase in the NBE is due to the reduction in the electron-hole recombination in the deep levels in the bandgap, while a second contribution is due to the formation of the shallow donor level due to interstitial hydrogen doping.

In order to explain the behavior of the NBE intensity, we can suppose that incorporation path (1) is dominant at the beginning of the treatment. When the as-prepared ZnO NRs are exposed to hydrogen plasma, the hydrogen atoms first interact with dangling bonds at the surface of the sample and by diffusion with oxygen and zinc vacancies inside the NRs, forming the complexes and by combination with OH groups leading to water desorption. This reduces the trapping of free electrons from deep level defects and results in an increased NBE intensity. A rough estimate of the order of magnitude of this effect can be deduced by the sample annealed at 300 °C in air for 1 h, which allows the reduction of the point defects and therefore of the DLE. A twofold increase in the NBE can also be observed in this annealed sample where no hydrogen doping is present. At a second stage, as the doping proceeds with incorporation path (2), since the point defects start being saturated by the complexes, the hydrogen atoms may penetrate into ZnO NRs as interstitial, H_i, increasing the bound exciton emission. This two-step behavior has already been observed in ZnO films doped with hydrogen in different concentrations produced by magnetron sputtering.[43] As the doping concentration increases, the band bending at the surface due to trapping of free electrons is reduced,[19] changing therefore the aspect ratio of the NRs, and the formation of other donor-like defects, such as Zn_i, is promoted.[43] Moreover, a high hydrogen doping concentration, as probably in the sample P-100, may also lead to higher microstrain in the crystal structure, as suggested by the broadening of the (002) diffraction in XRD [Fig. 1(e)]. All these effects can lead to a decrease in the NBE intensity without affecting the DLE, which is consistent with our PL measurements.

In order to support this interpretation of the doping process via APPJ, after the plasma treatment, the sample P-5 was further annealed in air at 300 °C for 1 h (P-5-Ann). The hydrogen doping process has been shown in the literature to be a reversible process at about 500 °C, due to hydrogen desorption.[42] The annealing at 300 °C aims to increase the mobility of the interstitial hydrogen without affecting the vacancy complexes. The PL results are shown in Fig. SI-3 and compared to the annealed-only and as-prepared samples. The NBE from the annealed P-5-Ann decreased to the magnitude of the annealed sample Ann-ZnO NRs: the heat process has therefore allowed the desorption of the H_i. On the other side, the passivation of the DLE is not affected by the annealing (Fig. SI-4), supporting the expected higher resistance of vacancy complexes to the temperature. In addition, if the NBE intensity increase was only due to the water desorption during the plasma process, the successive annealing would not have affected the NBE intensity. Also, this result suggests the doping description in two steps.

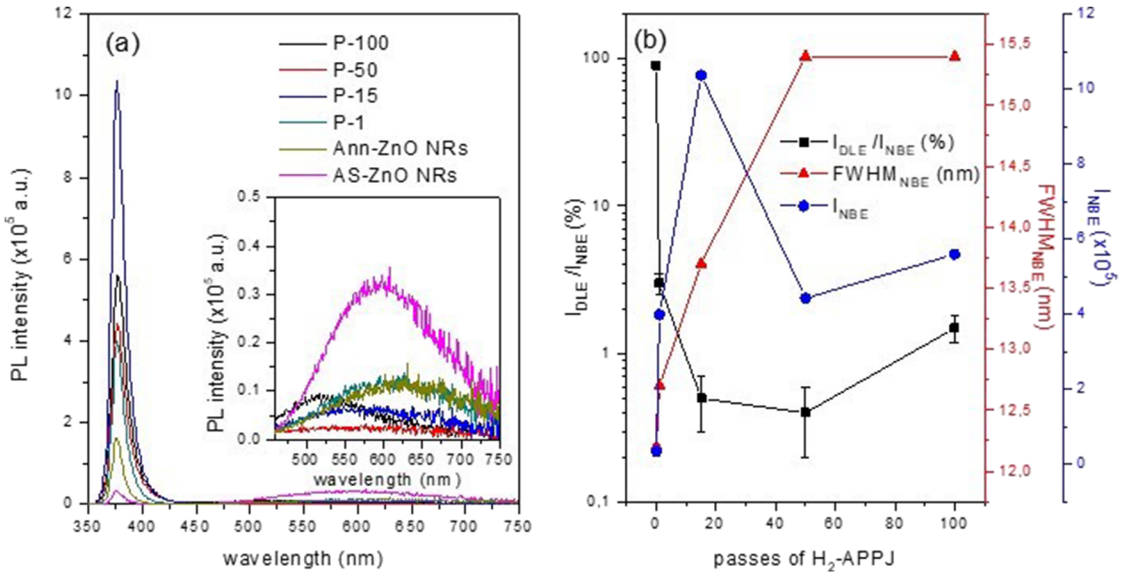

FIG. 3. (a) PL of reducing atmosphere APPJ treated ZnO NRs after exposure to UV for 30 min and about 2 months of aging. (b) Relative intensity and FWHM of PL vs the number of passes of APPJ treated samples after aging.

TABLE II. Evolution of PL profile vs APPJ treatments. The number in brackets refers to the error of the maximum I_{DLE} vs maximum I_{NBE}.

Sample	AS-ZnO	Ann-ZnO	P-1	P-15	P-50	P-100	P-5-Ann
I_{DLE}/I_{NBE} (%)	90 (5)	7 (1)	3.0 (0.5)	0.5 (0.2)	0.4 (0.2)	1.5 (0.3)	2.5 (0.5)
$FWHM_{NBE}$ (nm)	12.2	11.2	12.7	13.7	15.4	15.4	11.9

The stability of the process was verified after 2 months of aging [Fig. 3(a)]. After aging, the sample P-15 still showed the maximum NBE among all the samples, with an I_{NBE} increase to around 30 times, compared to the as-prepared sample. Compared to newly APPJ ZnO NRs, the DLE spectra from the samples after aging vary from each other. The P-100 sample has maximum visible emission around 525 nm, while the other samples have DLE centered around 600 nm. Figure 3(b) and Table II both show that after aging, the P-15, P-50, and P-100 samples preserved the broadened NBE peak profile and that visible emission was less than 2% of the NBE intensity. After aging, the relative FWHM of the NBE emission in sample P-15 is strongly reduced, approaching values close to the as-deposited ones, with the previous trend as a function of APPJ passes being less visible. Also, the thermal annealing of P-5 led to the same reduction. Therefore, the H_i may gradually diffuse out of the NRs reducing the stress of the microstructure.

C. Quantum efficiency (QE) of ZnO NRs

The steady-state PL showed an increase in the NBE intensity after the plasma treatment. However, whether the enhancement is due to the increase in light absorption or in emission efficiency from the absorbed light is still unknown. The fluorescence quantum efficiency (QE) was measured to clarify the matter.

Typically recorded ZnO spectra for QE calculation are shown in Fig. SI-1. The $Em_{FTO} = E_A$ is omitted in the QE calculation since the FTO emission is not visible in the ZnO emission spectra.

The photoluminescence QEs for different ZnO NR samples are calculated and plotted in Fig. 4. It is clear that QE_{NBE} (blue triangles) increases after annealing and is further enhanced after APPJ

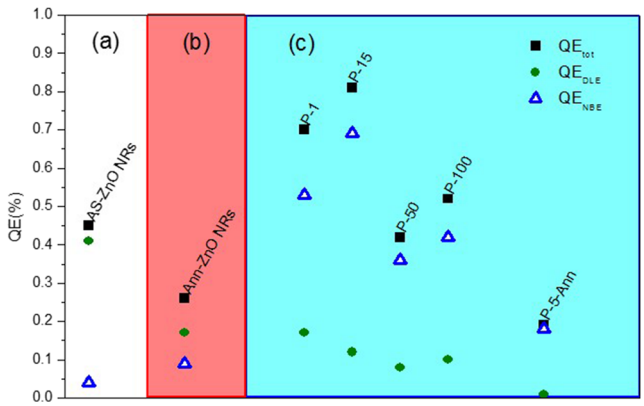

FIG. 4. The calculated QE for ZnO NRs after different treatments.

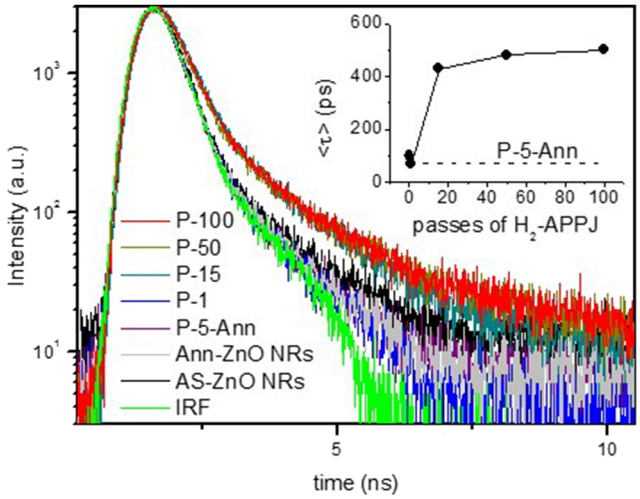

FIG. 5. Lifetime of NBE in ZnO NRs. IRF represents the instrument reference function. The inset collects the average decay of ZnO NRs' NBE vs the passes of H_2-APPJ. The dashed horizontal line refers to the lifetime of sample P-5-Ann.

treatments, while QE_{DLE} is reduced in all post-treated samples. All together, the APPJ treated samples result in a slightly improved total quantum efficiency QE_{tot} ($QE_{tot} = QE_{NBE} + QE_{DLE}$).

A similar measurement was performed on ZnO NRs; e.g., Gargas *et al.*[44] reported that the QE of ZnO is related to the morphology, defects in ZnO, temperature, and excitation power. The QE from our samples is very low, which is reasonable, considering the aspect ratio of the samples and the limited excitation power density (excitation from a Xe lamp and the light spot in the range of mm^2). However, the results show that even with low excitation power density, the plasma treated samples have much higher QE_{NBE} and that the increase in the treatment time with 50 and 100 passes does not further enhance QE_{NBE}. This effect is consistent with the NBE intensity behavior previously described, where an increase of the hydrogen doping level can be detrimental to the optical properties.

It can also be highlighted that the sample P-5-Ann showed a reduction in the $QE_{NBE,}$ but the QE_{DLE} did not recover to the level of the annealed samples. This evidence testifies again that the defects responsible for the DLE are effectively passivated by the hydrogen atoms.

D. Lifetime of ZnO NR UV-emission

The time-resolved PL intensity of ZnO nanostructures has been extensively studied in the literature, evidencing often a biexponential decay behavior,[14–17] with values ranging from tens to hundreds of picoseconds for the fast component (τ_1) and from hundreds of picoseconds to several nanoseconds for the long component (τ_2). The initial fast decay was attributed to the capture of excitons and carrier trapping by deep levels, followed by nonradiative relaxation processes,[45] while the slow component may be related to charge carrier trapping. The nanostructure morphology and crystalline quality also play an important role in the PL spectra and lifetime.[14,15] Moreover, bulk and surface states have different optical and lifetime characteristics, contributing to spectral and lifetime broadening. All these aspects, together with the lack of correlation between the PL emission intensity and the PL decay time for both the fast and slow processes of the biexponential decay indicate that different defects or defect complexes are involved in the processes responsible for the luminescence and carrier trapping followed by nonradiative relaxation.[14]

The time-resolved PL decay at 376 nm under 275 nm pulsed LED excitation is reported for our samples in Fig. 5. Annealing of ZnO NRs at 300 °C and light APPJ (P-1) does not change the decay of UV-emission. Increasing the number of plasma treatment passes results in broadening of NBE spectra, reduction in NBE QE, and longer NBE decay. Like most other ZnO nanostructures, deconvolution fitting of the measured lifetime data reveals that the τ_{PL} of our samples can be fitted by using a biexponential decay function.[14–17] The numerical results for the fitting parameters are reported in Table S1, evidencing a dominant role of the fast component. As previously discussed, several elements and defects are involved in the decay processes. Therefore, for comparison purposes, it is worth considering the average lifetime values, which are reported in Table III, calculated by using the following equation:[46]

$$\tau_{PL} = \frac{A_1\tau_1^2 + A_2\tau_2^2}{A_1\tau_1 + A_2\tau_2}, \quad (2)$$

where A_i and τ_i (i = 1, 2) are the amplitudes and lifetimes of the two fitting exponential decay components. The average τ_{PL} of the as-prepared sample is about 100 ps, while annealing induces a 10% reduction of this value. It is worth noting that the effect of plasma treatment is initially a 30% reduction of the lifetime, followed by a significant increase, up to 500 ps for the most intense plasma treatment (sample P-100).

In general, PL in ZnO consists of a band recombination process (NBE) and a radiative trap-related process (DLE). Additionally, nonradiative processes are also related to defects in the bulk structure. Our results show that a mild H_2-APPJ treatment like in P-1 is enough to passivate defects related to radiative DLE. Stronger treatments, from P-15 samples, can induce a deeper effect on the passivation of defects responsible for nonradiative recombinations, in agreement with the significant enhancement in NBE and the suppression in DLE in steady-state PL spectra. Compared to P-15, P-50 and P-100 have a slightly longer lifetime, while the QE_{NBE}

TABLE III. The average decay of ZnO NRs' NBE lifetime.

Sample	AS-ZnO NRs	Ann-ZnO NRs	P-1	P-15	P-50	P-100	P-5-Ann
τ_{PL} (ps)	100	80	70	430	480	500	70

and intensity of NBE decrease, which is probably attributed to the increasing interstitial hydrogen (H_i) in the ZnO NRs.

IV. CONCLUSIONS

In summary, we demonstrated the effect of atmospheric H_2-plasma treatment on the optical properties of hydrothermally synthesized ZnO NRs. The results show that H_2-plasma treatment at room temperature and under ambient air conditions (APPJ treatment) on ZnO NRs leads to an enhancement of the photoluminescence quantum efficiency (QE), attributed to the plasma process induced passivation of V_{Zn} that significantly suppresses the deep level emission (DLE). Moreover, an increase in the NBE was observed that is related to ZnO NR doping by the interstitial hydrogen (H_i), and the average lifetime increases due to the suppression of nonradiative recombination defects. All the results demonstrate that the action of the atmospheric pressure plasma is not related only to the activation and control of chemical functionalities at the surfaces, but it also allows doping in the bulk of the crystal. Moreover, the APPJ treatment induced stable enhancement in ZnO NR performance, which lasts even after exposure to UV irradiation and after keeping the sample in air for several months.

The high efficiency of the APPJ process and the possibility to apply it at room temperature and in an ambient environment make it a competitive alternative to heat treatment and vacuum plasma processes for the control of the conductivity and UV/Vis emissions of ZnO nanostructures. Moreover, it may find interesting applications also in the hydrogen doping of transparent conductive oxides on polymers.

SUPPLEMENTARY MATERIAL

See supplementary material for PL spectra recorded with an integrating sphere for QE calculation and PL of ZnO NRs under various conditions, including: no APPJ process, after aging, and after annealing. The numerical results of biexponential fitting of the NBE PL decay are also collected.

ACKNOWLEDGMENTS

S.J., P.G., F.E., and A.V. acknowledge the financial support from the Kempe Foundation, the ÅFORSK Foundation, the Knut and Alice Wallenberg Foundation, the Swedish Foundations consolidator fellowship, the European Union's Horizon 2020 research and innovation program under Grant Agreement No. 654002, and the Luleå University of Technology lab fund program. F.E. acknowledges financial support from VINNOVA through the Vinnmer Marie Curie Incoming—Mobility for Growth Programme (Project "Nano2solar" Ref. No. 2016-02011).

REFERENCES

[1] C. G. Van De Walle, "Hydrogen as a cause of doping in zinc oxide," Phys. Rev. Lett. **85**(5), 1012–1015 (2000).
[2] Ü Özgür, Y. I. Alivov, C. Liu *et al.*, "A comprehensive review of ZnO materials and devices," J. Appl. Phys. **98**(4), 1–103 (2005).
[3] Q. Peng and Y. Qi, "ZnO nanowires and their application for solar cells," in *Nanowires–Implementations and Applications*, edited by DAH (InTech, 2011).
[4] B. P. Yang, H. Yan, S. Mao *et al.*, "Controlled growth of ZnO nanowires and their optical properties," Adv. Funct. Mater. **12**(5), 323–331 (2002).
[5] N. Memarian, I. Concina, A. Braga, S. M. Rozati, A. Vomiero, and G. Sberveglieri, "Hierarchically assembled ZnO nanocrystallites for high-efficiency dye-sensitized solar cells," Angew. Chem., Int. Ed. **50**(51), 12321–12325 (2011).
[6] P. Ghamgosar, F. Rigoni, M. G. Kohan *et al.*, "Self-powered photodetectors based on core-shell ZnO-Co_3O_4 nanowire heterojunctions," ACS Appl. Mater. Interfaces **11**(26), 23454–23462 (2019).
[7] C. De Melo, M. Jullien, J. Ghanbaja *et al.*, "Local structure and point-defect-dependent area-selective atomic layer deposition approach for facile synthesis of p-Cu_2O/n-ZnO segmented nanojunctions," ACS Appl. Mater. Interfaces **10**(43), 37671–37678 (2018).
[8] C. de Melo, M. Jullien, Y. Battie *et al.*, "Semi-transparent p-Cu_2O/n-ZnO nanoscale-film heterojunctions for photodetection and photovoltaic applications," ACS Appl. Nano Mater. **2**, 4358 (2019).
[9] B. D. Yuhas and P. Yang, "Nanowire-based all-oxide solar cells," J. Am. Chem. Soc. **131**(13), 3756–3761 (2009).
[10] J. Cizek, J. Valenta, P. Hruska *et al.*, "Origin of green luminescence in hydrothermally grown ZnO single crystals," Appl. Phys. Lett. **106**, 251902 (2015).
[11] S. Baruah and J. Dutta, "Hydrothermal growth of ZnO nanostructures," Sci. Technol. Adv. Mater. **10**(1), 013001 (2009).
[12] S. Baruah, M. A. Mahmood, M. Tay, and Z. Myint, "Enhanced visible light photocatalysis through fast crystallization of zinc oxide nanorods," Beilstein J. Nanotechnol. **1**, 14–20 (2010).
[13] A. Janotti and C. G. V. D. Walle, "Fundamentals of zinc oxide as a semiconductor," Rep. Prog. Phys. **72**, 126501 (2009).
[14] W. M. Kwok, A. B. Djurišić, Y. H. Leung, W. K. Chan, and D. L. Phillips, "Time-resolved photoluminescence from ZnO nanostructures," Appl. Phys. Lett. **87**(22), 1–3 (2005).
[15] Y. Zhong, A. B. Djurišić, Y. F. Hsu *et al.*, "Exceptionally long exciton photoluminescence lifetime in ZnO tetrapods," J. Phys. Chem. C **112**(42), 16286–16295 (2008).
[16] T. Koida, S. F. Chichibu, A. Uedono *et al.*, "Correlation between the photoluminescence lifetime and defect density in bulk and epitaxial ZnO," Appl. Phys. Lett. **82**(4), 532–534 (2003).
[17] T. Koida, A. Uedono, A. Tsukazaki, T. Sota, M. Kawasaki, and S. F. Chichibu, "Direct comparison of photoluminescence lifetime and defect densities in ZnO epilayers studied by time-resolved photoluminescence and slow positron annihilation techniques," Phys. Status Solidi A **201**(12), 2841–2845 (2004).
[18] C. Chen, H. He, Y. Lu, K. Wu, and Z. Ye, "Surface passivation effect on the photoluminescence of ZnO nanorods," ACS Appl. Mater. Interfaces **5**(13), 6354–6359 (2013).
[19] J. Yoo, G. Yi, B. Chon, T. Joo, and Z. Wang, "Luminescence dynamics of bound exciton of hydrogen doped ZnO nanowires," J. Lumin. **176**, 278–282 (2016).
[20] J. Rodrigues, T. Holz, R. Fath Allah *et al.*, "Effect of N_2 and H_2 plasma treatments on band edge emission of ZnO microrods," Sci. Rep. **5**(1), 10783 (2015).
[21] S. Jiang, Z. Ren, S. Gong *et al.*, "Tunable photoluminescence properties of well-aligned ZnO nanorod array by oxygen plasma post-treatment," Appl. Surf. Sci. **289**, 252–256 (2014).
[22] A. Illiberi, B. Kniknie, J. van Deelen *et al.*, "Improved conductivity of ZnO thin films by exposure to an atmospheric hydrogen plasma," MRS Proc. **1447**, mrss12-1447-v04-03 (2012).
[23] L. E. Greene, B. D. Yuhas, M. Law, D. Zitoun, and P. Yang, "Solution-grown zinc oxide nanowires," Inorg. Chem. **45**(19), 7535–7543 (2006).
[24] A. Patelli, E. Verga Falzacappa, P. Scopece, R. Pierobon, and S. Vezzu', "Method for generating an atmospheric plasma jet and atmospheric plasma minitorch device," Wo2015071746 2(12) (2014).
[25] A. Patelli, F. Mussano, P. Brun *et al.*, "Nanoroughness, surface chemistry and drug delivery control by atmospheric plasma jet on implantable devices," ACS Appl. Mater. Interfaces **10**, 39512 (2018).
[26] P. Ghamgosar, F. Rigoni, S. You *et al.*, "ZnO-Cu_2O core-shell nanowires as stable and fast response photodetectors," Nano Energy **51**, 308–316 (2018).

[27]L. Vayssieres, "Growth of arrayed nanorods and nanowires of ZnO from aqueous solutions," Adv. Mater. **15**(5), 464–466 (2003).
[28]N. C. Das, S. Biswas, and P. E. Sokol, "The photovoltaic performance of ZnO nanorods in bulk heterojunction solar cells," J. Renewable Sustainable Energy **3**, 033105 (2011).
[29]R. Zhang, P. Yin, N. Wang, and L. Guo, "Photoluminescence and Raman scattering of ZnO nanorods," Solid State Sci. **11**(4), 865–869 (2009).
[30]C. F. Windisch, G. J. Exarhos, C. Yao, and L. Q. Wang, "Raman study of the influence of hydrogen on defects in ZnO," J. Appl. Phys. **101**(12), 123711 (2007).
[31]J. Lv and M. Fang, "Photoluminescence study of interstitial oxygen defects in ZnO nanostructures," Mater. Lett. **218**, 18–21 (2018).
[32]K. Vanheusden, W. L. Warren, C. H. Seager, D. R. Tallant, J. A. Voigt, and B. E. Gnade, "Mechanisms behind green photoluminescence in ZnO phosphor powders," J. Appl. Phys. **79**(10), 7983–7990 (1996).
[33]Y. Zhang and L. Zhang, "Effect of excitation intensity on fluorescence spectra in ZnO nanostructures and its origin," Sci. China, Ser. G: Phys., Mech. Astron. **52**(1), 4–12 (2009).
[34]U. Das and D. Mohanta, "Evolution of ZnO nanoparticles and nanorods: Aspect ratio dependent optoelectronic properties," Eur. Phys. J.: Appl. Phys. **53**(1), 10602 (2011).
[35]A. Y. Polyakov, N. B. Smirnov, A. V. Govorkov *et al.*, "Hydrogen plasma treatment effects on electrical and optical properties of n-ZnO," J. Appl. Phys. **94**(1), 400–406 (2003).
[36]M. D. McCluskey and S. J. Jokela, "Defects in ZnO," J. Appl. Phys. **106**(7), 071101 (2009).
[37]A. A. Mosquera, D. Horwat, A. Rashkovskiy *et al.*, "Exciton and core-level electron confinement effects in transparent ZnO thin films," Sci. Rep. **3**, 1714 (2013).
[38]Y. Li, M. Zhong, T. Tokizono, I. Yamada, G. Bremond, and J. J. Delaunay, "Stability of hydrogen incorporated in ZnO nanowires by plasma treatment," Nanotechnology **22**(43), 435703 (2011).
[39]P. F. Cai, J. B. You, X. W. Zhang *et al.*, "Enhancement of conductivity and transmittance of ZnO films by post hydrogen plasma treatment," J. Appl. Phys. **105**(8), 083713 (2009).
[40]L. J. Brillson, W. T. Ruane, H. Gao *et al.*, "Spatially-resolved cathodoluminescence spectroscopy of ZnO defects," Mater. Sci. Semicond. Process. **57**, 197–209 (2017).
[41]F. Oba, A. Togo, I. Tanaka, J. Paier, and G. Kresse, "Defect energetics in ZnO: A hybrid Hartree-Fock density functional study," Phys. Rev. B **77**(24), 245202 (2008).
[42]Y. M. Strzhemechny, J. Nemergut, P. E. Smith, J. Bae, D. C. Look, and L. J. Brillson, "Remote hydrogen plasma processing of ZnO single crystal surfaces," J. Appl. Phys. **94**(7), 4256–4262 (2003).
[43]D. Gaspar, L. Pereira, K. Gehrke, B. Galler, E. Fortunato, and R. Martins, "High mobility hydrogenated zinc oxide thin films," Sol. Energy Mater. Sol. Cells **163**, 255–262 (2017).
[44]D. J. Gargas, H. Gao, H. Wang, and P. Yang, "High quantum efficiency of band-edge emission from ZnO nanowires," Nano Lett. **11**, 3792 (2011).
[45]B. Guo, Z. Ye, and K. S. Wong, "Time-resolved photoluminescence study of a ZnO thin film grown on a (100) silicon substrate," J. Cryst. Growth **253**(1-4), 252–257 (2003).
[46]J. R. Lakowicz, *Principles of Fluorescence Spectroscopy* (Springer US, 1999).